J. Fluid Mech. (2014), *vol.* 756, *pp.* 452–469.
doi:10.1017/jfm.2014.470

Three-dimensional boundary layers with short spanwise scales

Richard E. Hewitt[1],† **and Peter W. Duck**[1]

[1]School of Mathematics, The University of Manchester, Oxford Road, Manchester M13 9PL, UK

(Received 5 February 2014; revised 19 June 2014; accepted 8 August 2014;
first published online 2 September 2014)

We investigate three-dimensional (laminar) boundary layers that include a spanwise scale comparable to the boundary-layer thickness. A forcing of short spanwise scales requires viscous dissipation to be retained in the two-dimensional cross-section, perpendicular to the external flow direction, and in this respect the flows are related to previous work on corner boundary layers. We use two examples to highlight the main features of this category of boundary layer: (i) a flat plate of narrow (spanwise) width, and (ii) a narrow (spanwise) gap cut into an otherwise infinite flat plate; in both cases the plate is aligned with a uniform oncoming stream. We find that a novel feature arises in connection with the external flow; the presence of a narrow gap/plate (or indeed any comparable short-scale feature of long streamwise extent) necessarily modifies the streamwise mass flux in that vicinity, which in turn induces an associated boundary-layer transpiration on the same short spanwise length scale. This (short-scale) transpiration region leads to a half-line-source/sink correction to the outer inviscid, irrotational flow. Crucially, the volumetric flux associated with this line-source/sink must be explicitly included as part of the computational procedure for the leading-order boundary layer, and as such there is a weak interaction between the outer (inviscid) flow and the boundary layer. This is a generic feature of boundary layers that are forced through the presence of short-scale spanwise variations.

Key words: boundary layers, boundary-layer structure

1. Introduction

Boundary-layer flows over surfaces with short-scale spanwise disturbances are a common feature in numerous applications, the most obvious being in aerodynamic settings. The ‘average’ wing/lifting surface of an aircraft exhibits numerous smooth and non-smooth variations, even close to a leading edge, some of which persist in the chord-wise direction. Diffusion of momentum in the cross-sectional plane is a dominant feature for such geometries, but the governing equations remain parabolic in the downstream coordinate. Such situations have been referred to as ‘three-dimensional parabolic flow’ by Patankar & Spalding (1972), Patankar (1980), and similar ‘longitudinally parabolised’ regions have arisen in compressible flows, as described by Neyland *et al.* (2008). This flow geometry presents a combination of analytical and computational difficulties, associated with viscous diffusion acting over

† Email address for correspondence: richard.e.hewitt@manchester.ac.uk

the entire downstream cross-section. The aim of this paper is to (i) better understand the physical effects, on an otherwise classical, two-dimensional laminar boundary layer, of deviations in surface characteristics that have spanwise scales comparable to the boundary-layer thickness, but have a large streamwise extent and (ii) present a rational and robust procedure for the computation of such flow states. One subclass of 'three-dimensional parabolic flow' that has aroused a significant amount of discussion is that of the flow near a streamwise-aligned semi-infinite corner formed by the intersection of two flat plates; this is strongly motivated by application to wing–body junctions. We first (briefly) review the existing material on corner boundary layers before focusing on the related class of flows that will form our current investigation.

The first theoretical study on streamwise-aligned corner boundary layers can be attributed to Carrier (1947), although it was subsequently pointed out by Kemp (1951) that not all momentum equations were satisfied in this formulation. Early attempts at obtaining numerical solutions to the problem were made by Loitsianskii & Bolshakov (1951) and Levy (1959). The development of singular perturbation theory in the 1960s enabled Rubin (1966) to develop the first asymptotically rigorous structure (in the limit of large Reynolds number), describing the blending of two boundary layers (one is extending in the spanwise direction, the other in the transverse direction). However, although the basic mathematical structure to the problem was then known, the numerical solution proved not to be straightforward, as evidenced by the differing published results of Rubin & Grossman (1969), Pal & Rubin (1971), Zamir (1973), Desai & Mangler (1974), Ghia (1975) and Zamir (1981). The work of Dhanak & Duck (1997) suggested that the imposition of (inaccurate) far-field boundary conditions on truncated domains was the likely culprit for these numerical disparities. A determination of the correct far-field constraints is a non-trivial issue in this class of flows, and is a topic that will be returned to in this work. Indeed, in investigating the far-field behaviour of this class of flow, it was noted by Ridha (1992) and Dhanak & Duck (1997) that in addition to the (expected) two-dimensional Blasius solution, an alternative, three-dimensional state also exists.

Over the years, experimental studies of corner flows have also been undertaken, including those by Zamir & Young (1970), Zamir & Young (1979), Zamir (1981), Barclay & El-Gamal (1983) and more recently Park *et al.* (2012). Most of these studies have been hot-wire based, owing to the inherent difficulties of visualising the small-scale spanwise features associated with the corner. However, the experiments collectively suggest that the laminar flow is highly sensitive to the form of the leading edge and to flow perturbations, which become unstable at significantly lower Reynolds numbers than for two-dimensional Blasius boundary layers. Dhanak & Duck (1997) and Lakin & Hussaini (1984) presented greatly simplified analyses, using quasi-parallel assumptions, although these studies did little to explain the disparity in stability characteristics between corner and (classical, two-dimensional) boundary-layer flows.

The primary difficulty in undertaking a proper stability analysis of such states, even assuming a streamwise parallel flow approximation, is the (strongly) two-dimensional nature of the base flow at a given downstream cross-section, leading to a 'biglobal' (i.e. 2D) eigenvalue problem (Theofilis 2003). Balachandar & Malik (1995) were the first to undertake a stability study of the two-dimensional base flow, although for the purposes of the stability analysis, they assumed infinite Reynolds number, leading to the two-dimensional analogue of the Rayleigh equation. An inclusion of viscous effects (and, hence, Reynolds number) into the stability equations was carried out by Parker & Balachandar (1999). Non-parallelism of the base flow has been incorporated,

using a parabolised stability equations approach by Galionis & Hall (2005), although this still did not explain the low stability threshold observed in experiments. In a more recent study, Alizard, Robinet & Rist (2010) hypothesised that the onset of an inflectional mechanism may be an explanation for this discrepancy.

A further paper, regarding the spatial (streamwise) development of corner boundary-layer flows, was Duck, Stow & Dhanak (1999), in which it was shown how the far field (and, hence, global) flow can be susceptible to algebraically growing spatial modes, related to those described by Luchini (1996); a key point to note is that classical Blasius flow is a case which exhibits such a mode. Duck, Stow & Dhanak (2000) showed that this type of 'instability' was not confined to corner flows, but is a quite generic feature found in boundary layers, with spanwise flow variations. Subsequently, the determination of 'optimal disturbances', i.e. the determination of the initial perturbations which lead to the maximum energy growth in Blasius-type boundary layers, has been considered by Luchini (2000) and Zuccher, Luchini & Bottaro (2004), the latter paper also incorporating nonlinear effects.

In this work we approach the same set of governing equations, as utilised in the aforementioned corner boundary-layer studies, which is a system that applies to any (high-Reynolds-number) flow in which viscous dissipation is of equal importance in both the spanwise and transverse directions, but change the context from the usual 'corner flows'.

The corner boundary-layer equations (despite the name) describe any (long) streamwise-aligned feature of sufficiently short spanwise scale. For example, this may be a short-scale variation in surface properties (e.g. wall transpiration or changes in the no-slip condition) or a surface deflection (e.g. a transverse ridge, or an additional boundary of finite transverse length that remains contained within the boundary layer). Herein we focus on two example problems that induce spanwise diffusion through a discontinuity in boundary conditions: (i) a flat plate of narrow (spanwise) width; and (ii) a narrow (spanwise) gap cut into an otherwise infinite flat plate, examining the solution in the neighbourhood of the plate edge.

In addition to being of interest in their own right, this class of flows constitutes an intermediate problem between (well-understood) classical boundary layers and (less-well-understood) corner boundary layers. As such, the mean flows we present may provide an alternative route for our developing understanding of the stability properties of comparable three-dimensional flows (such as corner flows), or indeed the more complex supersonic examples of the compensation regime of Neyland *et al.* (2008, § 8.2.2). However, as we shall address in detail below, even the computation of base flows that develop downstream in a self-similar manner requires careful consideration.

We begin by formulating the boundary-layer equations in § 2, maintaining diffusive effects in the cross-section. Appropriate boundary conditions at the base of the flow domain are provided in § 2, but the more complicated far-field constraints are outlined in § 3, where a computational formulation is presented. Results are presented that focus on the physical aspects of the flow in § 4. Non-uniqueness exists in these flows and § 5 provides some brief details of alternative solutions. We make some concluding remarks in § 6.

2. Boundary-layer formulation

We consider a flat plate placed at zero incidence into a uniform oncoming stream of a constant density incompressible fluid. The short-scale spanwise behaviour will be induced by allowing either the plate to have a 'narrow' gap (the axis of which

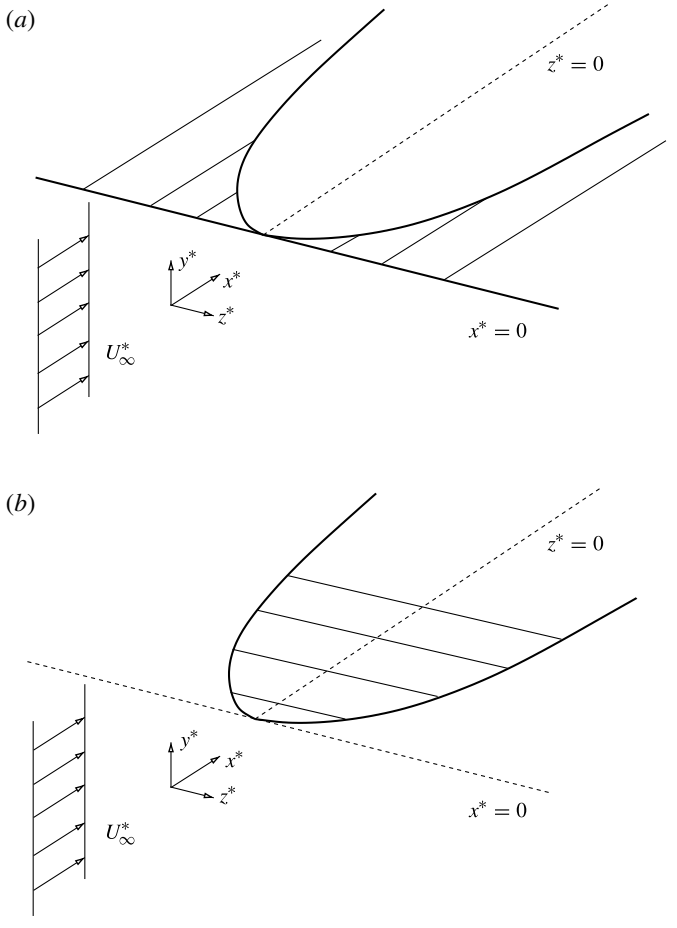

FIGURE 1. Schematic of the two flow domains: (*a*) a narrow gap in an otherwise semi-infinite plate; (*b*) a narrow plate. In both cases the plate is aligned with a uniform oncoming stream of speed U^*_∞ and the plate side edge is at $x^* = \pm F(x^*)$.

is aligned with the oncoming stream) or the plate width in the spanwise direction to be 'thin'. We use 'narrow' and 'thin' to indicate that the spanwise length scale is comparable with the (local) boundary-layer thickness in the transverse, y^*, direction. The asterisk superscript will be used to indicate dimensional quantities throughout this work. A schematic of the flow geometry is shown in figure 1.

In both cases shown in figure 1(*a*,*b*) there is a 'leading edge' at $x^* = 0$ and the gap/plate edge is defined by $z^* = \pm F(x^*)$ with a uniform oncoming flow of velocity U^*_∞ (there is no free-stream pressure gradient to leading order). The flow is described by a Cartesian coordinate system (x^*, y^*, z^*) with associated velocities (u^*, v^*, w^*), such that $z^* = 0$ is a line of symmetry and the flat-plate lies in the plane $y^* = 0$.

We may non-dimensionalise in the usual (Blasius-like) manner, seeking a solution in the form

$$(y^*, z^*) = \left(\frac{2x^*\nu^*}{U^*_\infty}\right)^{1/2} (\eta, \zeta), \tag{2.1a}$$

where this ζ scale is necessary to capture the short spanwise scales that will be of interest to us, with

$$u^* = U_\infty^* U(\zeta, \eta) + \cdots, \tag{2.1b}$$

$$(v^*, w^*) = \left(\frac{U_\infty^* \nu^*}{x^*}\right)^{1/2} (V(\zeta, \eta) + \cdots, W(\zeta, \eta) + \cdots). \tag{2.1c}$$

The associated (reduced) pressure field is

$$p^* = \rho^* {U_\infty^*}^2 \left[\left(\frac{\nu^*}{U_\infty^* x^*}\right)^{1/2} p_1 + \frac{\nu^*}{U_\infty^* x^*} p_2(\zeta, \eta) + \cdots\right], \tag{2.1d}$$

where ρ^* is the constant density, ν^* is the (constant) kinematic viscosity and p_1 is zero in the narrow plate case, but is a constant in the finite gap case (triggered by the Blasius boundary-layer displacement).

We make the usual boundary-layer approximation, under the assumption that the local Reynolds number $x^* U_\infty^*/\nu^*$ is large, and retain the leading-order terms. The resulting boundary-layer system retains viscous diffusion in the cross-sectional (constant x^*) plane owing to the length scales (2.1*a*). The leading-order system may be simplified by cross-differentiation to eliminate the pressure correction, p_2, and a slight change of dependent variables to Φ and Ψ, defined as follows

$$V(\zeta, \eta) = \frac{1}{\sqrt{2}}(\eta U(\zeta, \eta) - \Phi(\zeta, \eta)), \tag{2.2a}$$

$$W(\zeta, \eta) = \frac{1}{\sqrt{2}}(\zeta U(\zeta, \eta) - \Psi(\zeta, \eta)). \tag{2.2b}$$

The above formulation results in the well-known 'corner boundary-layer equations' (see Rubin 1966; Ghia 1975; Dhanak & Duck 1997, for example), in the form:

$$2U = \Phi_\eta + \Psi_\zeta, \quad \Theta = \Psi_\eta - \Phi_\zeta, \tag{2.3a,b}$$

and

$$\nabla^2 U = -\Phi U_\eta - \Psi U_\zeta, \tag{2.4a}$$

$$\nabla^2 \Theta = 2[\zeta U U_\eta - \eta U U_\zeta] - \Phi \Theta_\eta - \Psi \Theta_\zeta - 2U\Theta, \tag{2.4b}$$

and we can rewrite (2.3) as

$$\nabla^2 \Phi = 2U_\eta - \Theta_\zeta, \tag{2.4c}$$

$$\nabla^2 \Psi = 2U_\zeta + \Theta_\eta. \tag{2.4d}$$

Here ∇^2 is the two-dimensional Laplacian in the plane spanned by η and ζ. In what follows, we will solve the problem using the formulation (2.4).

To highlight the dominant features of our example problems, we will focus attention on cases where the edge of the plate is defined by $F(x^*) = \zeta_0(\nu^* x^*/U_\infty^*)^{1/2}$ for some coefficient ζ_0. This ensures that the spanwise length scale remains comparable to the (developing) transverse boundary-layer thickness at all locations downstream of the leading edge, and thus the similarity form is preserved. In terms of the rescaled boundary-layer coordinate, the edge of the plate then becomes $\zeta = \pm\zeta_0$.

2.1. *A narrow gap*

For the flow over a narrow gap, figure 1(*a*), the boundary conditions on $\eta = 0$ are

$$U = \Psi = \Phi = 0, \quad \Theta = \Psi_\eta, \quad \text{on } \eta = 0, \ \zeta \geqslant \zeta_0, \tag{2.5a}$$

arising from no-slip and impermeability of the plate, together with

$$U_\eta = \Psi_\eta = \Phi = \Theta = 0, \quad \text{on } \eta = 0, \ \ 0 \leqslant \zeta < \zeta_0, \tag{2.5b}$$

corresponding to a symmetric flow in the gap region. On assuming a reflectional symmetry about the $\zeta = 0$ axis, we are also required to impose

$$U_\zeta = \Phi_\zeta = \Psi = \Theta = 0, \quad \text{on } \zeta = 0, \ \ \eta \geqslant 0, \tag{2.5c}$$

and the far-field conditions will be introduced later.

2.2. *A narrow plate*

For the flow over a narrow plate, figure 1(*b*), the boundary conditions on $\eta = 0$ are modified to

$$U_\eta = \Psi_\eta = \Phi = \Theta = 0, \quad \text{on } \eta = 0, \ \ \zeta \geqslant \zeta_0, \tag{2.6a}$$

for a symmetric flow away from the plate, and

$$U = \Psi = \Phi = 0, \quad \Theta = \Psi_\eta, \quad \text{on } \eta = 0, \ \ 0 \leqslant \zeta < \zeta_0, \tag{2.6b}$$

for no-slip and impermeability of the plate. The conditions on $\zeta = 0$ remain as (2.5*c*).

3. A global computational formulation

Our task is to solve (2.4), subject to either (2.5) or (2.6) with suitable far-field constraints. The far-field behaviour naturally divides into a response free from short spanwise features (e.g. a Blasius boundary layer) plus a correction that is solely driven by the short-scale gap/plate. We mirror this approach in the governing equations by first rescaling based on the gap/plate 'width' ζ_0:

$$\zeta = \zeta_0 \hat{\zeta}, \tag{3.1a}$$

$$U(\zeta, \eta) = \hat{U}(\hat{\zeta}, \eta), \quad \Phi(\zeta, \eta) = \hat{\Phi}(\hat{\zeta}, \eta), \tag{3.1b}$$

$$\Psi(\zeta, \eta) = \zeta_0 \hat{\Psi}(\hat{\zeta}, \eta), \quad \Theta(\zeta, \eta) = \zeta_0 \hat{\Theta}(\hat{\zeta}, \eta), \tag{3.1c}$$

then seeking a (nonlinear) perturbation of the form

$$\hat{U} = U_B(\eta) + \tilde{U}(\hat{\zeta}, \eta), \tag{3.2a}$$

$$\hat{\Phi} = \Phi_B(\eta) + \tilde{\Phi}(\hat{\zeta}, \eta), \tag{3.2b}$$

$$\hat{\Psi} = \hat{\zeta} \Psi_B(\eta) + \tilde{\Psi}(\hat{\zeta}, \eta), \tag{3.2c}$$

$$\hat{\Theta} = \hat{\zeta} \Theta_B(\eta) + \tilde{\Theta}(\hat{\zeta}, \eta), \tag{3.2d}$$

where subscript 'B' indicates a known base solution that exists in the absence of any short spanwise scale forcing.

The perturbation quantities are governed by

$$\hat{\nabla}^2 \tilde{\Phi} = 2\tilde{U} - \tilde{\Theta}_{\hat{\zeta}}, \tag{3.3a}$$

$$\hat{\nabla}^2 \tilde{\Psi} = 2\zeta_0^{-2} \tilde{U}_{\hat{\zeta}} + \tilde{\Theta}_\eta, \tag{3.3b}$$

$$\hat{\nabla}^2\tilde{U} = -\Phi_B\tilde{U}_\eta - \tilde{\Phi}U'_B - \tilde{\Phi}\tilde{U}_\eta - \hat{\zeta}\Psi_B\tilde{U}_{\hat{\zeta}} - \tilde{\Psi}\tilde{U}_{\hat{\zeta}}, \tag{3.3c}$$

$$\begin{aligned}\hat{\nabla}^2\tilde{\Theta} = 2\left[\hat{\zeta}(U_B+\tilde{U})\tilde{U}_\eta + \hat{\zeta}\tilde{U}U'_B - \eta\zeta_0^{-2}(U_B+\tilde{U})\tilde{U}_{\hat{\zeta}}\right] \\ - (\Phi_B+\tilde{\Phi})\tilde{\Theta}_\eta - \hat{\zeta}\tilde{\Phi}\Theta'_B - \tilde{\Psi}(\Theta_B+\tilde{\Theta}_{\hat{\zeta}}) \\ - \hat{\zeta}\Psi_B\tilde{\Theta}_{\hat{\zeta}} - 2(U_B+\tilde{U})\tilde{\Theta} - 2\hat{\zeta}\tilde{U}\Theta_B,\end{aligned} \tag{3.3d}$$

where

$$\hat{\nabla}^2 \equiv \frac{\partial^2}{\partial\eta^2} + \frac{1}{\zeta_0^2}\frac{\partial^2}{\partial\hat{\zeta}^2}. \tag{3.3e}$$

The boundary conditions are obtained by substitution of (3.2) into (2.5) for the narrow gap problem, or (2.6) for the narrow plate problem; we do not explicitly restate them here.

3.1. *Far-field conditions for the boundary layer: $\eta \gg 1$ at fixed $\hat{\zeta}$*

The appropriate far-field conditions for the (leading-order) boundary-layer variables are

$$\tilde{\Phi} \sim \frac{A\eta}{\zeta_0^2\hat{\zeta}^2+\eta^2}, \tag{3.4a}$$

$$\tilde{\Psi} \sim \frac{A\hat{\zeta}}{\zeta_0^2\hat{\zeta}^2+\eta^2}, \tag{3.4b}$$

$$\tilde{U} = \tilde{\Theta} = 0, \tag{3.4c}$$

for $\zeta^2+\eta^2 \gg 1$ (where $\zeta = \zeta_0\hat{\zeta}$), away from any boundary. The coefficient A remains an unknown (*a priori*) that must be determined as part of the computational procedure. We will provide a physical interpretation of A in the Appendix to this paper; at this stage we simply note that it measures a mass flux towards ($A>0$) and away ($A<0$) the centreline $\eta=\zeta=0$ ($y^*=z^*=0$) in the cross-sectional plane (fixed x^*).

The computational domain is truncated at $\eta=\eta_\infty$ and $\hat{\zeta}=\hat{\zeta}_\infty$. If we naïvely impose (3.4) as Dirichlet conditions for arbitrary A, then the resulting solution is (in general) spurious, in the sense that it is not of boundary-layer type and will depend on the choice of domain truncation via η_∞ and $\hat{\zeta}_\infty$. This behaviour can be observed in figure 2, where solutions are clearly seen to be sensitive to η_∞ and $\hat{\zeta}_\infty$ at general values of A. However, there is a critical value of $A=A(\zeta_0)$ for which the solution is of boundary-layer type and independent of all arbitrary computational parameters. This state exists when the boundary layer is consistent with the correction to the outer flow (as discussed in the Appendix), and is shown in figure 2 as the solid lines. It is our assertion that this represents the 'true' value of A, triggered by the flow.

To obtain the interactive solution, for which A is determined as part of the process, we impose (3.4*b*) and (3.4*c*) as Dirichlet conditions along $\eta=\eta_\infty$, whilst (3.4*a*) is imposed as

$$\left.\frac{\partial\tilde{\Phi}}{\partial\eta}\right|_{\eta=\eta_\infty} = A\frac{\zeta_0^2\hat{\zeta}^2-\eta^2}{(\zeta_0^2\hat{\zeta}^2+\eta^2)^2}. \tag{3.5}$$

This 'softer' derivative condition for flow into/out of the domain, along with a similar treatment at the boundary $\hat{\zeta}=\hat{\zeta}_\infty$ (described below), allows A to be determined such that the solution is of boundary-layer type, that is it remains independent of the domain size.

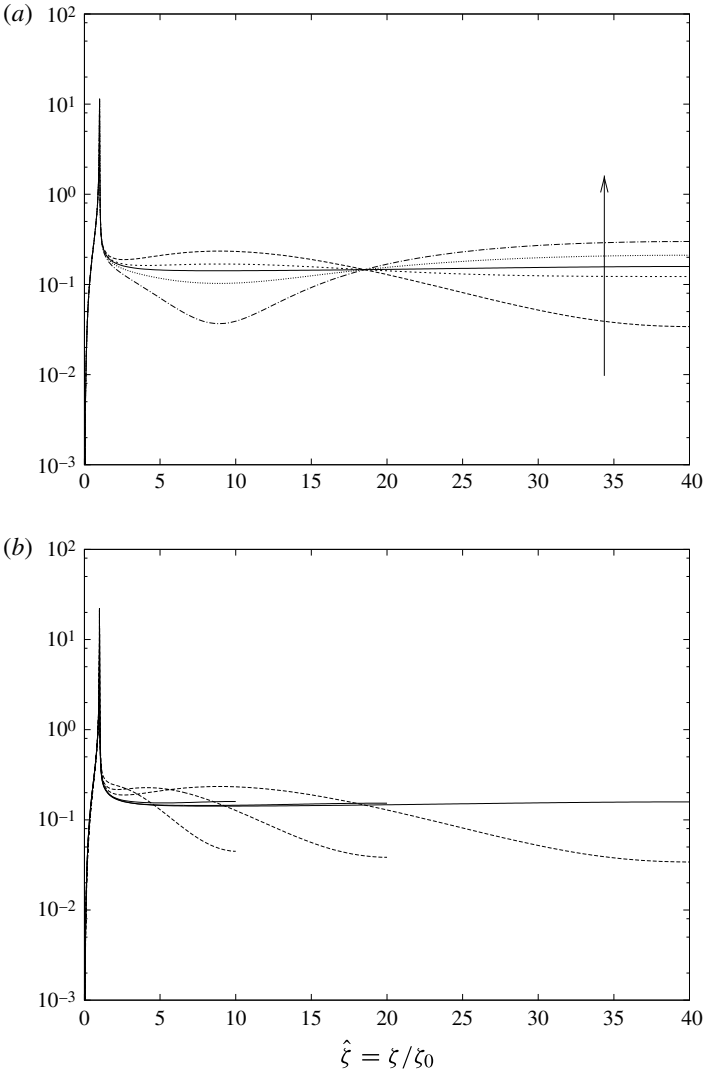

FIGURE 2. The variation of $\hat{\zeta}\tilde{\Theta}_\eta(\hat{\zeta}, \eta = 0)$ (off-plate, for $\hat{\zeta} < 1$) and $\hat{\zeta}\tilde{\Theta}(\hat{\zeta}, \eta = 0)$ (on-plate, for $\hat{\zeta} \geqslant 1$) in the case of the narrow gap problem with $\zeta_0 = 5$: (*a*) a fixed computational domain $\eta_\infty = \hat{\zeta}_\infty = 40$ with non-interacting 'solutions' evaluated with $A = 0$ (long dash), $A = 4$ (short dash), $A = 8$ (dotted) and $A = 12$ (dot–dash), increasing in the direction of the arrow shown; (*b*) non-interacting states at a fixed value of $A = 0$ (long dash) and increasing domain sizes, $\hat{\zeta}_\infty = \eta_\infty = 10$, 20, 40. In both (*a*) and (*b*) the analogous interacting solutions are also presented (solid lines), for which A is determined as part of the computational procedure; such states are clearly independent of arbitrary choices of computational domain size, unlike their non-interacting counterparts.

3.2. *Far-field conditions for the boundary layer:* $\hat{\zeta} \gg 1$*, a determination of* A

3.2.1. *A narrow plate*

For the geometry of a narrow plate, figure 1(*b*), the formulation is relatively straightforward as (3.4) remains valid for all η if $\hat{\zeta} \gg 1$. Along the boundary $\hat{\zeta} = \hat{\zeta}_\infty$

we impose (3.4*a*) and (3.4*c*) as Dirichlet conditions, whilst (3.4*b*) is imposed as

$$\left.\frac{\partial\tilde{\Psi}}{\partial\hat{\zeta}}\right|_{\hat{\zeta}=\hat{\zeta}_\infty} = \frac{A(\eta^2-\zeta_0^2\hat{\zeta}^2)}{(\zeta_0^2\hat{\zeta}^2+\eta^2)^2}, \tag{3.6}$$

and the additional unknown coefficient A is determined by the extra constraint

$$\zeta_0^2\hat{\zeta}_\infty\,\tilde{\Psi}(\hat{\zeta}_\infty,\,\eta=0)=A, \tag{3.7}$$

which follows from (3.4*b*).

3.2.2. *A narrow gap*

For a narrow gap in an otherwise infinite flat plate, as shown schematically in figure 1(*a*), the conditions to be imposed along $\hat{\zeta}=\hat{\zeta}_\infty$ are a little more involved, as (3.4) is not valid near to the plate, where viscous effects must be taken into account. For $\eta=O(1)$, a large-$\hat{\zeta}$ asymptotic solution exists in the form

$$\tilde{U} = A\bar{U}(\eta)/(\zeta_0^2\hat{\zeta}^2)+\cdots, \tag{3.8a}$$

$$\tilde{\Phi} = A\bar{\Phi}(\eta)/(\zeta_0^2\hat{\zeta}^2)+\cdots, \tag{3.8b}$$

$$\tilde{\Psi} = A\bar{\Psi}(\eta)/(\zeta_0^2\hat{\zeta})+\cdots, \tag{3.8c}$$

$$\tilde{\Theta} = A\bar{\Theta}(\eta)/(\zeta_0^2\hat{\zeta})+\cdots. \tag{3.8d}$$

Therefore, the leading-order functional form for the (nonlinear) perturbation induced by the short spanwise scale features can be determined from a (sixth-order) one-dimensional boundary-value problem for $(\bar{U},\bar{\Phi},\bar{\Psi},\bar{\Theta})$ subject to $\bar{U}=\bar{\Phi}=\bar{\Psi}=0$ on $\eta=0$ and $\bar{U},\,\bar{\Theta}\to 0,\,\bar{\Psi}\to 1$ as $\eta\to\infty$.

Rather than imposing (3.8), which is only valid for $\eta=O(1)$, we instead construct composite solutions for $\tilde{\Psi}$ and $\tilde{\Phi}$ using (3.4) and (3.8):

$$\tilde{\Psi} \sim \frac{A}{\zeta_0^2}\left\{\frac{\bar{\Psi}(\eta)}{\hat{\zeta}}-\frac{\eta^2}{\hat{\zeta}(\zeta_0^2\hat{\zeta}^2+\eta^2)}\right\}, \tag{3.9a}$$

$$\tilde{\Phi} \sim \frac{A}{\zeta_0^2}\left\{\frac{\bar{\Phi}(\eta)}{\hat{\zeta}^2}-\frac{\eta^3}{\hat{\zeta}^2(\zeta_0^2\hat{\zeta}^2+\eta^2)}\right\}. \tag{3.9b}$$

The boundary conditions imposed at $\hat{\zeta}=\hat{\zeta}_\infty$ are then

$$\hat{\zeta}\tilde{U}_{\hat{\zeta}}+2\tilde{U}=0, \tag{3.10a}$$

$$\hat{\zeta}\tilde{\Phi}_{\hat{\zeta}}+2\tilde{\Phi}=\frac{2A\eta^3}{(\zeta_0^2\hat{\zeta}^2+\eta^2)^2}, \tag{3.10b}$$

$$\hat{\zeta}\tilde{\Psi}_{\hat{\zeta}}+\tilde{\Psi}=\frac{2A\eta^2\hat{\zeta}}{(\zeta_0^2\hat{\zeta}^2+\eta^2)^2}, \tag{3.10c}$$

$$\hat{\zeta}\tilde{\Theta}_{\hat{\zeta}}+\tilde{\Theta}=0. \tag{3.10d}$$

In this case, as (3.7) is trivially satisfied by the no-slip constraint, we therefore determine the volume flux coefficient A by the analogous constraint

$$\zeta_0^2\hat{\zeta}_\infty\,\tilde{\Theta}(\hat{\zeta}_\infty,\,\eta=0)=A\bar{\Theta}(0), \tag{3.11}$$

which follows from (3.8*d*).

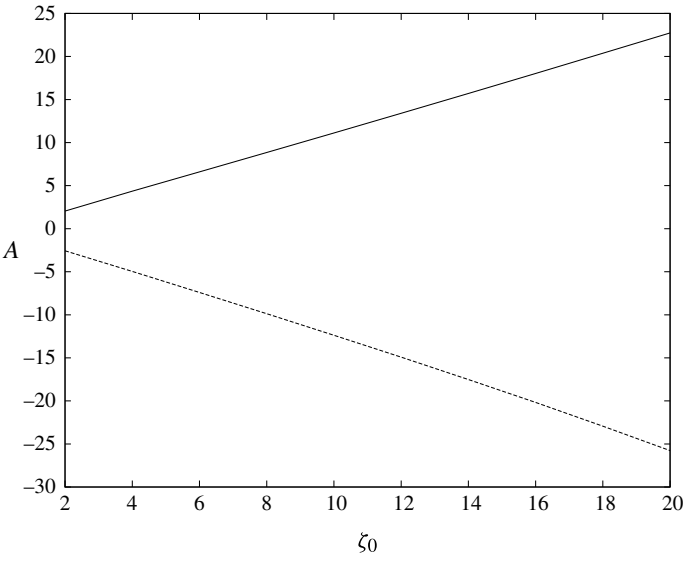

FIGURE 3. Evolution of the volumetric flux amplitude, A, as induced by the short spanwise scales for increasing gap/plate width parameter ζ_0. The upper solid line corresponds to the narrow-gap problem, where the gap acts as a half-line sink ($A > 0$) in the outer inviscid flow. The lower dashed line corresponds to the narrow-plate problem, where the plate acts as a half-line source ($A < 0$) in the outer inviscid flow.

4. Numerical results

The computational scheme employs a uniformly spaced computational mesh of $N_1 \times N_2$ points in the $(\bar{\zeta}, \bar{\eta})$-plane where $\bar{\zeta} = \bar{\zeta}(\hat{\zeta})$, $\bar{\eta} = \bar{\eta}(\eta)$, $0 \leqslant \hat{\zeta} \leqslant \hat{\zeta}_\infty$ and $0 \leqslant \eta \leqslant \eta_\infty$. The two functions $\bar{\zeta}$ and $\bar{\eta}$ are chosen to concentrate more nodal points near the boundary $\eta = 0$ and in the gap/edge region $\hat{\zeta} \leqslant 1$ when viewed in the original $(\hat{\zeta}, \eta)$ plane. The resulting system of $4N_1N_2 + 1$ equations (the coefficient A, is an additional unknown) is linearised about a current guess, and Newton iteration is applied to determine the corrections. At each iteration the (sparse) linear system is solved using the SuperLU library (Demmel *et al.* 1999). Typical computational values are $\hat{\zeta}_\infty = 20$, $\eta_\infty = 60$ and $N_1 = N_2 = 401$, leading to approximately 6.4×10^5 degrees of freedom; all results presented in figures below are independent of these computational parameters and the spacing functions $\bar{\zeta}(\hat{\zeta})$ and $\bar{\eta}(\eta)$.

Here we present results for both cases, of a narrow gap and a narrow plate. In the former problem, the underlying base flow (in the absence of any short-scale forcing by the presence of a narrow gap) is simply the two-dimensional Blasius solution; that is, $U_B = F'(\eta)$, $\Phi_B = F(\eta)$, $\Psi_B = F'(\eta)$ and $\Theta_B = F''(\eta)$ in (3.2) where

$$F''' + FF'' = 0, \tag{4.1}$$

with $F(0) = 0$, $F'(0) = 0$ and $F'(\eta_\infty) = 1$. For the latter problem, the underlying base flow (in the absence of the short-width plate) is merely $U_B = 1$, $\Phi_B = \eta$, $\Psi_B = 1$ and $\Theta_B = 0$. These are the natural choices, but not the only possibilities, as we shall briefly discuss in § 5 later.

Figure 3 shows the dependence of the coefficient A in (3.4) on the parameter ζ_0, which quantifies the width of the gap in figure 1(*a*) and the width of the plate in

figure 1(*b*). As noted earlier (see also the Appendix), A is a measure of the mass transfer induced in the cross-sectional plane. A gap in an otherwise infinite plate acts as a sink in the cross-sectional plane, that is $A > 0$, whilst a narrow-plate in an undisturbed uniform flow acts as a source, $A < 0$. In both cases the volumetric flux induced by the gap/plate increases with the gap/plate width, ζ_0, and our numerical results suggest that $A \sim \zeta_0$ for large ζ_0.

In figure 4 we show the flow field for both the narrow-gap (left) and narrow-plate (right) geometries, for two representative values of $\zeta_0 = 4$ and $\zeta_0 = 8$. Figure 4(*a*,*c*,*e*,*g*) show trajectories that are everywhere tangential to the in-plane velocity field (V, W) as defined by (2.1*b*). Figure 4(*b*,*d*,*f*,*h*) show contours of the corresponding streamwise velocity U. For clarity, figure 4 shows only a portion of the larger computational domain (that with the most interesting flow structure).

A narrow gap in an otherwise semi-infinite plate leads to an associated half-line sink behaviour ($A > 0$) in the far-field, as described by (3.4). However, the underlying (Blasius) base flow leads to a uniform transpiration in the far-field. Away from the plate, the Blasius solution dominates and the flow is still out of the boundary layer and into the free stream, as shown in figure 4(*a*,*c*). However, within the boundary layer the radial inflow induced by the narrow gap can dominate near to $\eta = \hat{\zeta} = 0$, which is also visible in these same figures. The edge of the plate acts as sink in the cross-sectional plane, and the size of this region in the transverse (η) direction is increased for increasing gap size ζ_0. This increase in transverse displacement thickness is clearly visible by comparing figure 4(*a*,*c*). As the gap widens, we also observe that the streamwise flow essentially becomes uniform $U \approx 1$ on the centreline $\hat{\zeta} = 0$.

For the problem of a narrow plate, the reduction in streamwise velocity induced by the no-slip constraint on the plate induces a source flow in the cross-sectional plane, $A < 0$. Because the underlying base flow is the trivial uniform (streamwise) flow, this source is clearly evident in the trajectories of figure 4(*e*,*g*). The off-plate streamwise motion returns to $U \approx 1$ rapidly, as seen in figure 4(*f*,*h*).

In both geometries we can examine the solution at the centreline/mid-plane, $\hat{\zeta} = \eta = 0$, for increasing values of the gap/plate width parameter ζ_0. Figure 5(*a*) shows the dependence of the streamwise velocity on ζ_0 for the narrow-gap problem. As expected, the streamwise velocity along the centreline U ($\zeta = 0$, $\eta = 0$) rapidly approaches the free-stream value of unity as the gap is widened. However, for increasing gap sizes, the resulting flow near $\zeta = 0$ is not simply the uniform flow found in the free stream (as perhaps might be anticipated), as can be seen from the dependence of $\tilde{\Psi}_{\hat{\zeta}}$ ($\hat{\zeta} = 0$, $\eta = 0$). In terms of the cross-flow defined by (2.2):

$$W \sim \frac{\zeta}{\sqrt{2}}(\tilde{U}(\hat{\zeta} = 0, \eta = 0) - \tilde{\Psi}_{\hat{\zeta}} \ (\hat{\zeta} = 0, \eta = 0)) \tag{4.2}$$

for small ζ. Therefore, a difference in $\tilde{U}$ and $\tilde{\Psi}_{\hat{\zeta}}$ at $\hat{\zeta} = 0$ corresponds to a locally three-dimensional flow.

A similar situation occurs for the narrow-plate problem, as shown in figure 5(*b*). For increasing plate width (that is, ζ_0 increasing), the centreline streamwise shear (U_η evaluated at $\hat{\zeta} = \eta = 0$) does not approach that of a Blasius boundary layer. Similarly the difference in the two components still points to a locally three-dimensional flow.

5. Alternative solutions

If we consider the example of a narrow gap in an otherwise semi-infinite flat plate, the substitution (3.2) decomposes the solution into a (base flow) component

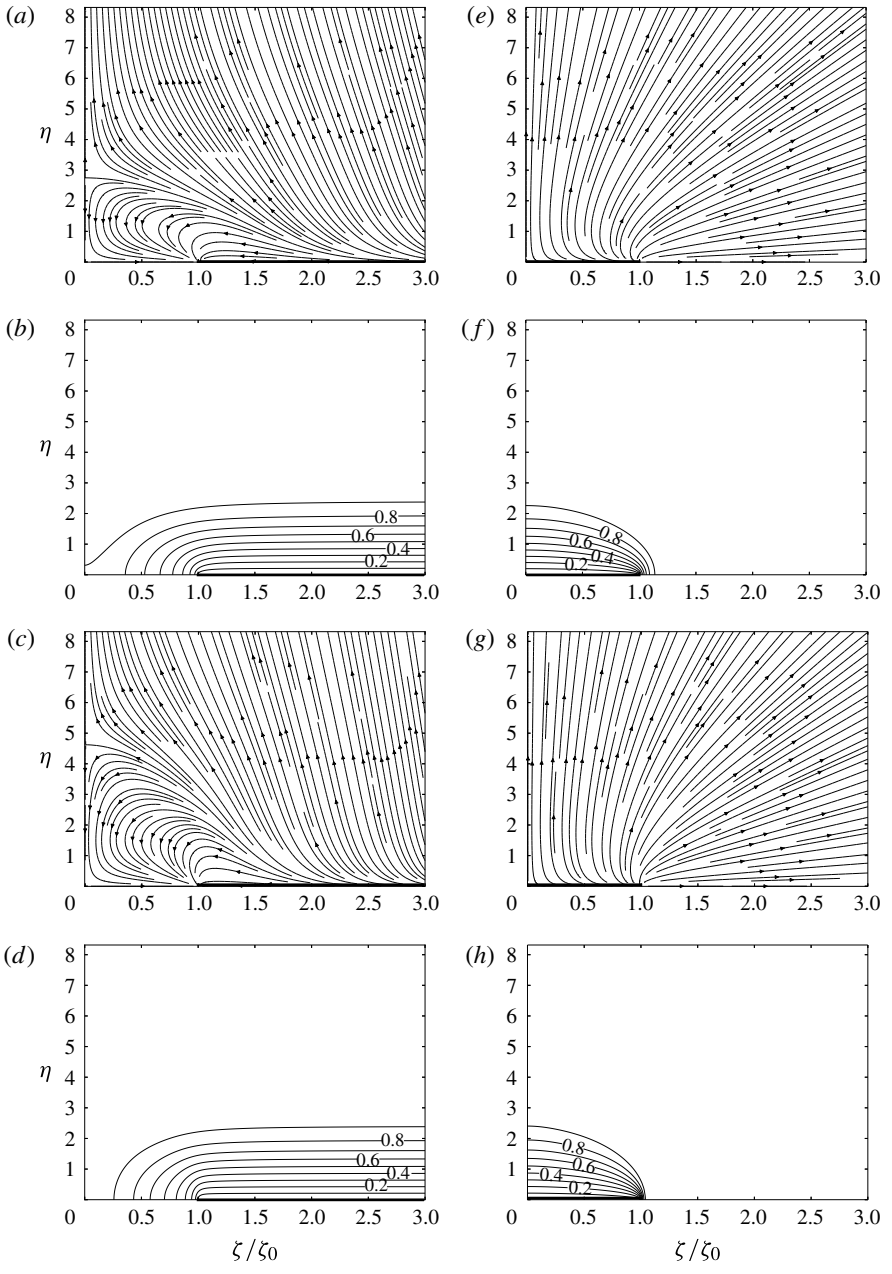

FIGURE 4. Left-hand column is the narrow gap problem: (*a*) the cross-sectional (V, W) velocity field for $\zeta_0 = 4$; (*b*) contours of downstream speed U for $\zeta_0 = 4$; (*c*) the cross-sectional (V, W) velocity field for $\zeta_0 = 8$; (*d*) contours of downstream speed U for $\zeta_0 = 8$. Right-hand column is the narrow plate problem: (*e*) the cross-sectional (V, W) velocity field for $\zeta_0 = 4$; (*f*) contours of downstream speed U for $\zeta_0 = 4$; (*g*) the cross-sectional (V, W) velocity field for $\zeta_0 = 8$; (*h*) contours of downstream speed U for $\zeta_0 = 8$. Only part of the full computational domain is shown.

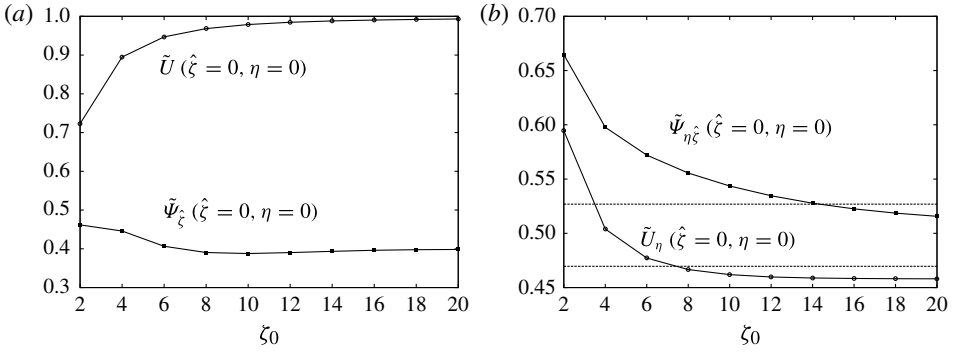

FIGURE 5. (*a*) The narrow-gap problem: evolution of the centreline mid-gap quantities U and $\tilde{\Psi}_{\zeta}$ for increasing gap width ζ_0. (*b*) The narrow-plate problem: evolution of the centre mid-plate shear quantities $\tilde{U}_{\eta}$ and $\tilde{\Psi}_{\eta\zeta}$ for increasing gap width ζ_0. In (*b*), the lower dashed line indicates the shear coefficient for a two-dimensional Blasius boundary layer (0.4696), whilst the upper dashed line shows the analogous three-dimensional alternative base flow that is discussed in § 5.

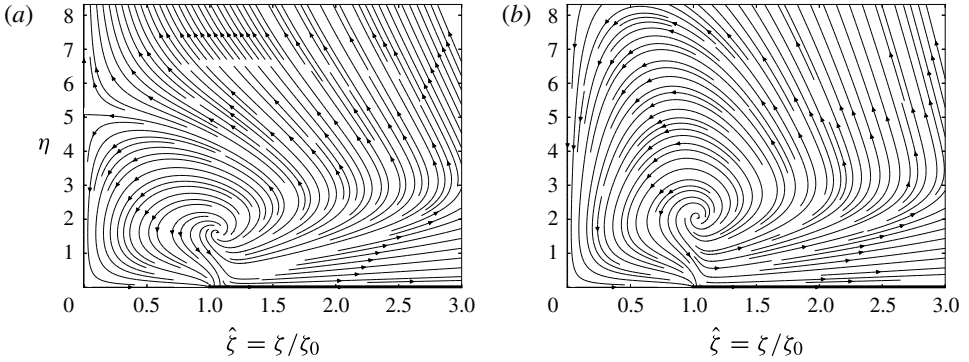

FIGURE 6. Results for the three-dimensional alternative to a Blasius base flow: the cross-sectional (V, W) velocity field for (*a*) $\zeta_0 = 4$, and (*b*) $\zeta_0 = 8$. Only part of the full computational domain is shown.

that solves the governing system in the absence of any gap, plus a correction that is solely due to the short-scale spanwise forcing (i.e. the gap). In this case, the obvious two-dimensional base flow solution is that due to Blasius, however, as noted above, this is not the only solution. As discussed by Ridha (1992) and Dhanak & Duck (1997), there is an alternative three-dimensional analogue to the classical Blasius solution and the reader is referred to those papers for further details.

On choosing U_B, Φ_B, Ψ_B and Θ_B in (3.2) to correspond to this three-dimensional alternative to Blasius, the nature of the flow response in the narrow-gap problem changes somewhat. In figure 6 we recompute solutions in the same manner and present the vector field in the cross-sectional plane of constant x for $\zeta_0 = 4, 8$. The qualitative features of figure 6(*a*) are to be compared with figure 4(*a*), as obtained for the classical two-dimensional Blasius base flow with the same gap width $\zeta_0 = 4$; similarly figure 6(*b*) can be compared with figure 4(*c*) for $\zeta_0 = 8$. Contours of the

streamwise velocity are qualitatively similar to those of figure 4 and, in the interests of brevity, we do not include them for this alternative solution.

These alternative states remain isolated from those of figure 4 for any ζ_0, however we note that the two states can be made to interact on the inclusion of a downstream pressure gradient; we do not pursue this broader problem here.

Similar alternative (two-dimensional) base flows can be obtained for the narrow plate problem. We do not pursue such states here on the basis that, even in the absence of short-scale spanwise forcing, they have algebraic decay of vorticity into the free stream; see for example Brown & Stewartson (1965) and Hewitt, Duck & Stow (2002) for further discussion of such behaviour.

6. Discussion

In this work we have considered a class of boundary-layer flows that have a short-scale spanwise forcing over a length scale $\Delta^* \sim (\nu^* x^*/U_\infty^*)^{1/2} \ll 1$. The exact nature of this forcing is not significant to the qualitative conclusions of this work (obviously quantitative details will vary). As specific examples we consider the flow over a semi-infinite flat plate that contains a narrow-width gap, or a narrow-width plate (as illustrated schematically in figure 1). In both cases the plate is taken to be in an otherwise uniform free-stream flow with zero pressure gradient.

The salient feature of these flows is that when the gap width (or plate width), and therefore Δ^*, is comparable to the transverse boundary-layer thickness δ^* (at any downstream position), viscous diffusion of momentum must be retained in both the transverse and spanwise directions. It is of some significance to note that the same general features can be found in many other (related) configurations, for example, any short-scale spanwise variations in surface boundary conditions (via changes to topography, transpiration or no-slip constraints). Some of these cases have appeared in the literature in Duck *et al.* (2000) (a spanwise ridge of short scale) and Zuccher *et al.* (2004) (a spanwise transpiration of short scale) and further examination of the far-field boundary conditions imposed in such cases is perhaps warranted in the light of our current results.

A short spanwise scale ridge is also considered by Neyland *et al.* (2008, (8.2.2)) in the context of surface roughness elements. We should note that the 'longitudinally parabolised' equations that arise in region 3 of their work ultimately lead to our governing system (2.4), even though their work is aimed at compressible flows. Our results also offer support for their assumption that disturbances persist over a transverse distance comparable to the roughness width.

The physical mechanism that is associated with these flows is an intuitive one. Any forcing of a boundary layer on a spanwise length scale of Δ^* will lead to a modification of the transverse flow into (or out of) the exterior flow over this same length scale. In the outer flow this additional transpiration from the boundary layer will induce a correction, which on the $O(1)$ spanwise length scale will appear as a line source/sink centred at the position of the short-scale forcing. In the general parabolic problem, the relative strength of this source/sink will be a function of the downstream position, as Δ^*/δ^* will in general vary downstream unless the forcing preserves this ratio as herein. This mechanism would be of little significance if its only influence was to contribute a high-order correction to the otherwise uniform flow of the outer inviscid solution. However, near the location of the forcing the magnitude of the source/sink flow must be included in the far-field boundary conditions for the boundary-layer velocities (see Appendix). A failure to include the correct far-field

behaviour leads to results that depend on arbitrary computational parameters owing to an incorrect prediction of the mass flux in the cross-sectional domain (as shown in figure 2).

We expect such flows to be of relevance in any situation where sufficiently short-scale spanwise features exist within the boundary layer for a finite distance in the downstream direction. However, they are also of interest in that they offer non-trivial three-dimensional solutions of the corner boundary-layer equations that can be smoothly connected to the well-known Blasius state (for the narrow gap problem) as $\zeta_0 \to 0$. In this context they may be a suitable test problem for future stability analyses; as noted earlier, the stability properties of the full corner boundary-layer problem are, as yet, to be fully established. In this regard, we should note that the spatial stability of these flows to downstream developing perturbations is unknown, similarly the parabolic marching of solutions (from a region near the leading edge) in cases for which Δ^*/δ^* is a function of downstream position remains a problem of current interest. In the immediate vicinity of a leading edge, we should expect a full Navier–Stokes region; indeed the predictions for the far-field behaviour discussed in the Appendix rely on being away from this zone with $x \gg y, z$.

We conclude by noting that an obvious limit to consider is $\Delta^*/\delta^* \to \infty$, where the spanwise length scale becomes long compared with the local transverse boundary-layer thickness. In the context of our example problems herein, this limit is $\zeta_0 \gg 1$. As mentioned in § 4, for the geometry of figure 1(*a*), as the gap width increases ($\zeta_0 \to \infty$) one may expect the in-gap flow (i.e. near $\zeta = 0$) to approach the undisturbed state ($U = 1$, $\Phi = \eta$, $\Psi_\zeta = 1$, $\Theta_\zeta = 0$). Likewise in the case of the finite-width plate, as $\zeta_0 \to \infty$, the corresponding assumption would be that, sufficiently close to $\zeta = 0$, the flow can be described by the classical Blasius equation. However, our numerical results above suggest that these assumptions are naïve for gap widths or plate widths that are of $O(\zeta_0(\nu^* x^*/U_\infty)^{1/2})$ as $\zeta_0 \to \infty$. One might still expect these assumptions to ultimately be appropriate for gap/plate sizes that are sufficiently large compared to the transverse boundary-layer thickness, but if this is the case, the flow states must arise beyond an intermediate regime.

As ζ_0 increases, we find that $A \sim \zeta_0$ and there remains an $O(1)$-width region around the plate-edge $\zeta = \zeta_0$, in which spanwise diffusion is important. A similar $O(1)$-width region develops around $\zeta = 0$. In this $O(1)$ centreline region the flow remains diffusive in ζ and does not locally resemble known solutions of uniform flow (narrow gap), or Blasius' solution (narrow plate). In this context it is worth noting that the work of Stewartson (1961) and Duck & Hewitt (2012) show that the flow in the vicinity of a 'quarter-infinite' plate has an unusual structure. This is because the outer flow for the quarter-plate geometry induces a spanwise length scale of $O(\Delta^* \log(U_\infty^* x^*/\nu^*))$, which is long compared with the $O(\Delta^*)$ scales considered in this work. Therefore, the limit of $\zeta_0 \gg 1$ in the current formulation remains distinct from the quarter-plate formulation.

Appendix A. Matching to an irrotational outer flow

When there is a narrow gap in a flat plate (for example), the no-slip conditions are replaced by transverse symmetry conditions in the gap. We therefore expect a relative increase in the streamwise flow in this region. Such an increased downstream volume flux must be replaced either laterally from the on-plate boundary layer, and/or from the free-stream flow. An accurate description of this crucial feature is necessary to obtain a boundary layer that is consistent with the correction to the outer potential flow. Perhaps surprisingly, this induced volume flux must also be explicitly included

in the solution process for the leading-order boundary-layer system when formulated with short spanwise scales.

In the established manner, Van Dyke (1964), in the outer (irrotational) inviscid solution, we seek a dimensionless velocity potential $\phi(x, y, z)$ where ϕ and (x, y, z) are made dimensionless with respect to some length scale L^* and the free-stream velocity U^*_∞. The velocity potential must satisfy Laplace's equation in the fluid subject to a weak transverse flow induced by the boundary layer on $y = 0$:

$$\left.\frac{\partial \phi}{\partial y}\right|_{y\to 0, x>0} = Re^{-1/2}x^{-1/2}\left(v_B + \bar{v}(\zeta, \eta \to \infty)\right), \tag{A 1}$$

where $Re = U^*_\infty L^*/\nu^*$. For the geometry of figure 1(*a*), v_B is the usual (constant) transpiration coefficient associated with a two-dimensional (Blasius) boundary layer on a semi-infinite plate. For the geometry of figure 1(*b*) there is no displacement in the absence of the narrow plate and therefore $v_B = 0$. The term $\bar{v}$ represents an additional (non-constant) transverse velocity induced over the short spanwise scales. At this stage $\bar{v}$ is unknown, but its general form is constrained by the matching process, as we shall discuss below.

We can decompose the (outer) velocity potential solution into a uniform-flow component, a two-dimensional correction, and a further contribution induced by the short spanwise scales:

$$\phi(x, y, z) = x + \phi_B(x, y) + \bar{\phi}(x, y, z), \tag{A 2}$$

where the subscript B indicates the two-dimensional outer solution in the absence of any short-scale spanwise forcing within the boundary layer. From the above, obviously ϕ_B and v_B are identically zero in the case of the narrow-plate problem, but they are non-zero in the narrow-gap problem.

Our interest lies with the contribution $\bar{\phi}$, for which a Green's function solution for the induced outer flow follows by standard methods:

$$\bar{\phi} = -\frac{1}{2\pi}\int_{X=0}^{\infty}\int_{Z=-\infty}^{\infty} Re^{-1/2}x^{-1/2}\frac{\bar{v}(\bar{\zeta}, \eta \to \infty)}{\sqrt{(x-X)^2 + y^2 + (z-Z)^2}}\,\mathrm{d}X\,\mathrm{d}Z, \tag{A 3}$$

where $\bar{\zeta} = ZRe^{1/2}/(2x)^{1/2}$, which is equivalent to (2.1*a*), but for the integration variable. As the induced transpiration $\bar{v}$ is a function of the short spanwise scale ζ, on the longer outer scale this appears as a volume flux from the half-line $x > 0$, $y = z = 0$ and the above integral can be reduced to a leading-order expression:

$$\bar{\phi} \sim -\frac{M}{\pi\sqrt{2}Re}\int_{X=0}^{\infty}\frac{1}{\sqrt{(x-X)^2 + y^2 + z^2}}\,\mathrm{d}X, \tag{A 4}$$

where M is a dimensionless measure of the volumetric out/in-flow of the line source/sink,

$$M = \int_{\bar{\zeta}=0}^{\infty}\bar{v}(\bar{\zeta}, \eta \to \infty)\,\mathrm{d}\bar{\zeta}. \tag{A 5}$$

Evaluation of the integral (A 4) yields the leading-order velocity potential for the correction due to the presence of the small-scale spanwise features,

$$\bar{\phi} \sim \frac{M}{\pi\sqrt{2}Re}\log\left(\sqrt{x^2 + y^2 + z^2} - x\right); \tag{A 6}$$

which is merely the velocity potential solution for a semi-infinite line source/sink.

A computation of the velocity components in the cross-sectional plane now leads to

$$\frac{\partial \phi}{\partial y} \sim \frac{\partial \phi_B}{\partial y} + \frac{M\sqrt{2}}{\pi Re}\frac{y}{y^2+z^2}, \tag{A 7a}$$

$$\frac{\partial \phi}{\partial z} \sim \frac{M\sqrt{2}}{\pi Re}\frac{z}{y^2+z^2}, \tag{A 7b}$$

for $y, z \ll x$. The terms proportional to Re^{-1} are (typically) of higher order. However, on approaching the short-scale region of the gap/plate near $y = z = 0$, they form a (leading-order) far-field contribution to the boundary layer when $y, z = O(x^{1/2}Re^{-1/2})$, which are the relevant scales of § 2. In this formulation the volumetric flux M is unknown *a priori* and must be determined in conjunction with the leading-order viscous boundary layer, and as such there is an interaction between the inviscid outer flow and the boundary layer.

REFERENCES

ALIZARD, F., ROBINET, J.-C. & RIST, U. 2010 Sensitivity analysis of a streamwise corner flow. *Phys. Fluids* **22**, 014103.

BALACHANDAR, S. & MALIK, M. R. 1995 Inviscid instability of streamwise corner flow. *J. Fluid Mech.* **282**, 187–202.

BARCLAY, W. H. & EL-GAMAL, H. A. 1983 Streamwise corner flow with wall suction. *AIAA J.* **21** (1), 31–37.

BROWN, S. N. & STEWARTSON, K. 1965 On similarity solutions of the boundary-layer equations with algebraic decay. *J. Fluid Mech.* **23** (04), 673–687.

CARRIER, G. F. 1947 The boundary layer in a corner. *Q. Appl. Maths* **4** (4), 367–370.

DEMMEL, J. W., EISENSTAT, S. C., GILBERT, J. R., LI, X. S. & LIU, J. W. H. 1999 A supernodal approach to sparse partial pivoting. *SIAM J. Matrix Anal. Applics.* **20** (3), 720–755.

DESAI, S. S. & MANGLER, K. W. 1974 Incompressible laminar boundary layer flow along a corner formed by two intersecting planes. *RAE Technical Report* 74062.

DHANAK, M. R. & DUCK, P. W. 1997 The effects of freestream pressure gradient on a corner boundary layer. *Proc. R. Soc. Lond.* A **453** (1964), 1793–1815.

DUCK, P. W. & HEWITT, R. E. 2012 A resolution of Stewartson's quarter-infinite plate problem. *Theor. Comput. Fluid Dyn.* **26** (1–4), 117–140.

DUCK, P. W., STOW, S. R. & DHANAK, M. R. 1999 Non-similarity solutions to the corner boundary-layer equations (and the effects of wall transpiration). *J. Fluid Mech.* **400** (1), 125–162.

DUCK, P. W., STOW, S. R. & DHANAK, M. R. 2000 Boundary-layer flow along a ridge: alternatives to the Falkner–Skan solutions. *Phil. Trans. R. Soc. Lond.* A **358** (1777), 3075–3090.

GALIONIS, I. & HALL, P. 2005 Spatial stability of the incompressible corner flow. *Theor. Comput. Fluid Dyn.* **19** (2), 77–113.

GHIA, K. N. 1975 Incompressible streamwise flow along an unbounded corner. *AIAA J.* **13** (7), 902–907.

HEWITT, R. E., DUCK, P. W. & STOW, S. R. 2002 Continua of states in boundary-layer flows. *J. Fluid Mech.* **468**, 121–152.

KEMP, N. H. 1951 The laminar three-dimensional boundary layer and a study of the flow past a side edge. MAeS thesis, Cornell University.

LAKIN, W. D. & HUSSAINI, M. Y. 1984 Stability of the laminar boundary layer in a streamwise corner. *Proc. R. Soc. Lond.* A **393** (1804), 101–116.

LEVY, R. 1959 The boundary layer in a corner. PhD thesis, Princeton University.

LOITSIANSKII, L. G. & BOLSHAKOV, V. P. 1951 On the motion of fluid in the boundary layer near the line of intersection of two planes. *NACA Tech. Mem.* 1308 (Translation).

LUCHINI, P. 1996 Reynolds-number-independent instability of the boundary layer over a flat surface. *J. Fluid Mech.* **327**, 101–116.

LUCHINI, P. 2000 Reynolds-number-independent instability of the boundary layer over a flat surface: optimal perturbations. *J. Fluid Mech.* **404** (1), 289–309.

NEYLAND, V. YA., BOGOLEPOV, V. V., DUDIN, G. N. & LIPATOV, I. I. 2008 *Asymptotic Theory of Supersonic Viscous Gas Flows*. Butterworth-Heinemann.

PAL, A. & RUBIN, S. G. 1971 Asymptotic features of viscous flow along a corner. *Q. Appl. Maths* **29**, 91–108.

PARK, D. H., PARK, S. O., KWON, K. J. & SHIM, H. J. 2012 Particle image velocimetry measurement of laminar boundary layer in a streamwise corner. *AIAA J.* **50** (4), 811–817.

PARKER, S. J. & BALACHANDAR, S. 1999 Viscous and inviscid instabilities of flow along a streamwise corner. *Theor. Comput. Fluid Dyn.* **13** (4), 231–270.

PATANKAR, S. V. 1980 *Numerical Heat Transfer and Fluid Flow*. CRC Press.

PATANKAR, S. V. & SPALDING, D. B. 1972 A calculation procedure for heat, mass and momentum transfer in three-dimensional parabolic flows. *Intl J. Heat Mass Transfer* **15** (10), 1787–1806.

RIDHA, A. 1992 On the dual solutions associated with boundary-layer equations in a corner. *J. Engng Maths* **26** (4), 525–537.

RUBIN, S. G. 1966 Incompressible flow along a corner. *J. Fluid Mech.* **26** (pt 1), 97–110.

RUBIN, S. G. & GROSSMAN, B. 1969 Viscous flow along a corner: numerical solution of corner layer equations. Polytechnic Institute of Brooklyn, Department of Aerospace Engineering and Applied Mechanics.

STEWARTSON, K. 1961 Viscous flow past a quarter-infinite plate. *J. Aero. Sci.* **28**, 1–10.

THEOFILIS, V. 2003 Advances in global linear instability analysis of non-parallel and three-dimensional flows. *Prog. Aerosp. Sci.* **39** (4), 249–315.

VAN DYKE, M. 1964 *Perturbation Methods in Fluid Mechanics,* vol. 964. Academic Press.

ZAMIR, M. 1973 Further solution of the corner boundary-layer equations. *Aeronaut. Q.* **24**, 219–226.

ZAMIR, M. 1981 Similarity and stability of the laminar boundary layer in a streamwise corner. *Proc. R. Soc. Lond.* A **377** (1770), 269–288.

ZAMIR, M. & YOUNG, A. D. 1970 Experimental investigation of the boundary layer in a streamwise corner. *Aeronaut. Q.* **21**, 313–339.

ZAMIR, M. & YOUNG, A. D. 1979 Pressure gradient and leading edge effects on the corner boundary layer. *Aeronaut. Q.* **30**, 471–484.

ZUCCHER, S., LUCHINI, P. & BOTTARO, A. 2004 Algebraic growth in a Blasius boundary layer: optimal and robust control by mean suction in the nonlinear regime. *J. Fluid Mech.* **513**, 135–160.